Biosensors and Bioelectronics 139 (2019) 111325

Contents lists available at ScienceDirect

Biosensors and Bioelectronics

journal homepage: www.elsevier.com/locate/bios

# Photoelectrochemical biosensor of HIV-1 based on cascaded photoactive materials and triple-helix molecular switch

Shaopeng Wang[a], Jinge Zhao[a], Yan Zhang[a], Mei Yan[b], Lina Zhang[c,*], Shenguang Ge[a,**], Jinghua Yu[b]

[a] Collaborative Innovation Center of Technology and Equipment for Biological Diagnosis and Therapy in Universities of Shandong, Institute for Advanced Interdisciplinary Research, University of Jinan, Jinan, Shandong, 250022, PR China
[b] School of Chemistry and Chemical Engineering, University of Jinan, Jinan, Shandong, 250022, PR China
[c] Shandong Provincial Key Laboratory of Preparation and Measurement of Building Materials, School of Material Science and Engineering, University of Jinan, Jinan, 250022, PR China

ARTICLE INFO

*Keywords:*
Cascaded photoactive materials
Triple-helix molecular switch
Microfluidic paper-based analytical device
HIV-1

ABSTRACT

In this work, an ultrasensitive photoelectrochemical (PEC) biosensor was proposed to detect nucleic acids on the basis of cascaded photoactive materials and triple-helix molecular switch. DNA sequence of human immunodeficiency virus type 1 (HIV-1) was chosen as the target DNA (T-DNA). Cascaded photoactive structure was formed via different sizes of CdTe quantum dots (QDs) sensitized ZnO nanorods (ZnO NRs), which was employed as a cascaded photoactive interface to amplify the photocurrent signal. A hairpin structure DNA (H-DNA) as capture probe was conjugated onto the photoactive interface through amide bond, and then a single-stranded DNA modified with gold nanoparticles labeled alkaline phosphatase (ALP-Au NPs-DNA) at each end was introduced to hybridize with the H-DNA to form a triple-helix conformation. The T-DNA detection was based on the photocurrent response change resulted from conformation change of the triple-helix molecule after hybridization with T-DNA. In the absence of T-DNA, the triple-helix molecule was in a closed state and the ALP of ALP-Au NPs-DNA could specifically catalyze the ascorbic acid 2-phosphate (AAP) to generate ascorbic acid (AA) as electron donors, which resulted in a significant photocurrent response due to the rapid electron transfer process. However, in the presence of T-DNA, the T-DNA hybridized with the ALP-Au NPs-DNA molecule, which caused triple-helix molecule in an opened state and compelled ALP-Au NPs-DNA away from the electrode surface, resulting in the absence of ALP which could catalyze AAP to generate AA. Subsequently, the photocurrent response significantly decreased. The proposed PEC biosensor not only had a wide detection range of 1fM-1nM and low detection limit (0.65 fM), but also showed excellent reproducibility, specificity and stability, which had great application prospect and opened up a new research method in the early clinical diagnosis and cancer research.

## 1. Introduction

Nucleic acids are important genetic information carrier in living organisms. It plays a role in storing and transmitting genetic information in life activities, and determines a series of major life phenomena such as growth, inheritance and variation of organisms (Sauna and Kimchi-Sarfaty, 2011). Therefore, accurate, rapid and specific nucleic acid assays have become a central issue in modern life sciences for gene therapy, clinical diagnosis and cancer research (Chen et al., 2011; Ito et al., 2007). In the past decade, various kinds of biosensors for nucleic acids detection have been reported, such as electrochemistry (Ge et al., 2016; Liu et al., 2014), electrochemiluminescence (Chai et al., 2010; Zhang et al. 2009, 2013), fluorescence (Hu et al., 2014; Huang et al., 2012; Li et al., 2013) and colorimetry (Baeissa et al., 2010; Ma et al., 2012; Zhang et al., 2010). Among these DNA biosensors, although they have their own advantages, they also have the defects of low sensitivity, long analysis time and complicated equipment (Darain et al., 2003). Photoelectrochemical (PEC) biosensors have become a novel analytical method with great potential application due to high sensitivity, simple equipment and easy miniaturization (Haddour et al., 2006).

PEC biosensor as a newly emerging and promising analytical method, which includes two processes of photoelectric conversion and

* Corresponding author.
** Corresponding author.
*E-mail addresses:* zhanglina818@126.com (L. Zhang), chm_gesg@163.com (S. Ge).

https://doi.org/10.1016/j.bios.2019.111325
Received 27 February 2019; Received in revised form 25 April 2019; Accepted 12 May 2019
Available online 16 May 2019
0956-5663/ 

electrochemistry (Shu et al., 2018; Zhao et al., 2018). Benefitting from the separation of the excitation source and electrochemical detection signal, PEC biosensors have been widely used in the bioanalysis, such as glutathione analysis (Tang et al., 2013), DNA analysis (Fan et al., 2014; Li et al., 2015; Zang et al., 2014), cell correlation analysis (Li et al. 2016, 2017) and immunoassay (Fan et al., 2016; Lan et al., 2016). In recent years, with the increasing research of PEC biosensors, photoactive materials that can be used for PEC analysis have also attracted extensive attention, photoactive materials are critical in the performances of the PEC biosensors. ZnO nanomaterial was widely utilized as the basic photoactive material in the construction of PEC biosensors due to the unique stability, faster charge transfer rate and better biocompatibility (Zhang et al., 2014). However, the further application is limited because of the wide band gap of ZnO (Feng et al., 2017). To achieve further improvement of photocurrent intensity, the other narrow band gap semiconductor materials were needed to sensitize ZnO (Zhang et al., 2017). Quantum dots (QDs) have attracted substantial research interest due to their own advantages of nanoscale size, tunable emission spectra and good biocompatibility (Gill et al., 2008). Qian and coworkers used CdS and $TiO_2$ to form a photoelectric conversion layer to increase the photocurrent density, and achieved the detection of target protein (Qian et al., 2010). However, up to now, few reports on the cascade structure strategy of different sizes of QDs to enhance the photocurrent signal of biosensors. The emission spectrum of the QDs could be controlled by changing its size. In this work, a photoactive interface with cascade band-edge level was formed via different sizes of QDs sensitized ZnO NRs, which could enhance the capture of light energy and improve the photoelectric conversion efficiency (Lee et al., 2010). In view of the above advantages, the design of photoactive interface is an ideal method for constructing PEC biosensors due to significant signal amplification.

Triple-helix molecular switch as a novel research method has been received much attention (Patterson et al., 2010; Wang et al., 2014). Wang et al. reported a signal-on and label-free electrochemical DNA biosensor by utilizing the triple-helix DNA structure with a high sensitivity (Wang et al., 2015). The triple-helix structure is universally applicable in biosensors due to its independent property of binding sequence. We can freely alter the sequence without change the triple-helix structure to detect any targets. Compared with the traditional double-helix DNA structure, the triple-helix molecular structure strategy has some obvious superiority. For example, the triple-helix structure has better stability than that of double- helix DNA and leaves more targets sequence, which can enhance the specificity and binding affinity to the targets, thereby achieving much higher sensitivity (Zheng et al., 2012). However, as far as we know, the triple-helix molecular switch strategy has not been reported in the PEC biosensor until now.

Herein, an ultrasensitive and high specificity PEC biosensor was fabricated based on the cascaded photoactive materials and triple-helix molecular switch. The DNA sequence of human immunodeficiency virus type 1 (HIV-1) was selected as target DNA (T-DNA). As shown in Scheme 1, firstly, ZnO NRs were attached onto the gold-paper working electrode (Au-PWE) of microfluidic paper-based analytical device (μ-PAD) (Fig. S1) and were sensitized by CdTe-COOH QDs (QDs1) and CdTe-$NH_2$ QDs (QDs2) to form a cascaded photoactive interface. A hairpin structure DNA as capture probe (H-DNA) was immobilized on the QDs2/QDs1/ZnO/Au-PWE through the amide bond, 6-mercaptohexanol (MCH) was used to block non-specific sites. Then, a single-stranded DNA modified with gold nanoparticles labeled alkaline phosphatase (ALP-Au NPs-DNA) at each end was introduced to hybridize with H-DNA to form a triple-helix conformation. Ascorbic acid 2-phosphate (AAP) could be specifically catalyzed by ALP to generate ascorbic acid (AA) as electron donors, which could provide electrons to combine with photo-generated holes of electrode surface and enhance the photocurrent signal evidently. When the T-DNA existed, T-DNA hybridized with ALP-Au NPs-DNA of the triple-helix molecule to disassemble the triple-helix conformation, which made the H-DNA to recover to its original structure and forced the ALP-Au NPs-DNA to leave the electrode surface, thereby reducing the photocurrent signal. Herein, a signal-off PEC biosensor for HIV-1 detection was fabricated. Most importantly, the designed biosensor had good versatility, which could specifically bind different target molecules by changing the sequence of ALP-Au NPs-DNA to achieve the detection of multiple targets.

## 2. Experimental section

### 2.1. Synthesis of ZnO NRs

Typically, 0.44 g of $Zn(COOH)_2{\cdot}2H_2O$ were dissolved in 10 mL of ethanolamine under stirring to form a transparent solution. Subsequently, 5 mL of water and 15 mL of ethylene glycol were added to the solution to obtain mixed solution and sonicated for 30 min. The solution was transferred into a steel-lined Teflon autoclave (100 mL capacity) and put it into a blast drying oven. The autoclave was sealed and heated to 180 °C for 4 h. After the reaction, it was cooled to room temperature in the air. Finally, the precipitate was centrifuged and rinsed with anhydrous ethanol and distilled water several times to remove the residuum, and dried under vacuum for 12 h.

### 2.2. Synthesis of different sizes of CdTe QDs

The synthetic method of different sizes of CdTe QDs was based on previous reports with some modifications (see the supplementary material) (Fan et al., 2014).

### 2.3. Preparation of ALP-Au NPs-DNA conjugates

The preparation process of ALP -Au NPs-DNA conjugates was according to the previous methods with some modifications (Zhao et al., 2012). Firstly, 0.2 M $K_2CO_3$ were added dropwise into the gold nanoparticles (Au NPs) solution to adjust the pH to 8.2 under stirring. Secondly, DNA (20 μL, 1 μM) (DNA sequences are shown in Table S1) and ALP (40 μL, 0.8 mg/mL) were added successively into 2.0 mL of Au NPs solution for 2 h. Afterward, the non-specific active sites were blocked with 200 μL of MCH solution (2 mM) for 30 min at room temperature. Next, the mixture was centrifuged at 10,000 rpm for 20 min and washed several times with the washing buffer to remove the residues. Finally, the precipitate was dissolved in 200 μL of distilled water to obtain ALP-Au NPs-DNA conjugates.

### 2.4. Fabrication of the PEC biosensor

The preparation process of the PEC biosensor for the detection of T-DNA was provided in the supplementary material.

### 2.5. PEC detection

PEC detection was performed at room temperature in PBS solution (pH 7.4, 0.1 M) containing 0.1 M AAP, which was used as a precursor of electron donors during the photocurrent signal measurement. The white light produced by the Xe lamp as the light source and was switched on and off every 10 s. The applied potential was 0.0 V. The obtained PEC biosensor incubated with different concentration of T-DNA.

## 3. Results and discussion

### 3.1. Characterization of Au-PWE and ZnO NRs

As shown in Fig. 1A, the surface of the bare paper electrode was the cellulose fiber with a porous structure, which provided an outstanding adsorption microenvironment for the loading of gold seeds. As displayed in Fig. 1B and C, Au NPs modified the PWE was fabricated via a

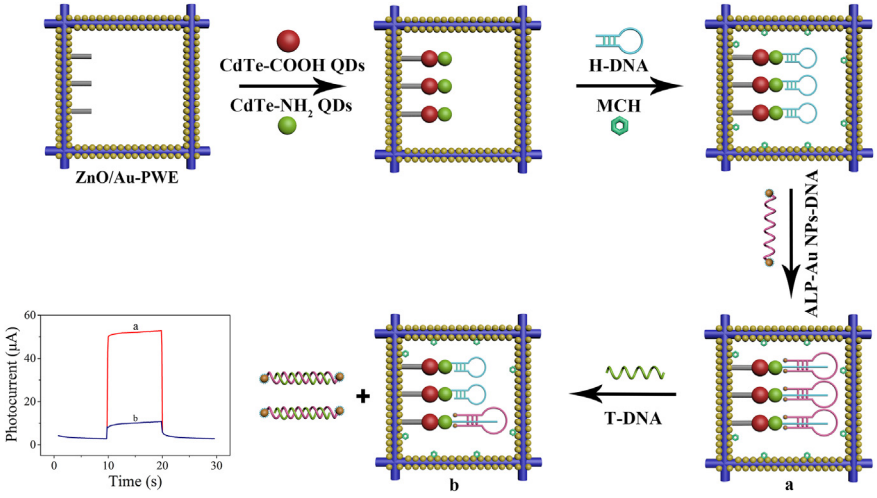


**Scheme 1.** The fabrication process of the PEC biosensor for detection of HIV-1.

self-catalytic reduction process of Au NPs growth and a continuous and uniform conductive Au NPs layer was successfully obtained on the surface of the paper fibers. Scanning electron microscope (SEM) image of the ZnO NRs modified Au-PWE was showed in Fig. 1D, from which we could obviously observe that the ZnO arrays were composed of independent ZnO NRs and perpendicular growth on the electrode surface. The magnified SEM image in Fig. 1E showed that the ZnO NRs had a hexagonal structure, which possessed a large surface area and provided an outstanding carrier for the attachment of QDs1. In addition, X-Ray Diffraction (XRD) was used to prove the successful preparation of the ZnO NRs. Fig. 1F showed the XRD of ZnO NRs, no characteristic peaks from other impurities were detected, indicating the high purity of the as-synthesized ZnO NRs.

### 3.2. Characterization of QDs1 and QDs2

The transmission electron microscope (TEM) images and ultraviolet-visible (UV-vis) absorption spectra were used to characterize the prepared CdTe QDs. Fig. 2A and B showed the TEM images of the prepared QDs1 and QDs2, respectively. The particle sizes were acquired to be approximately 3.7 nm and 2.3 nm from the TEM images, respectively. As shown in Fig. 2C and D, for QDs1, the spectrum showed a broad absorption range below 610 nm and an evident absorption peak located at 571 nm, the spectrum of QDs2 exhibited an absorption range below 575 nm and an obvious absorption peak located at 506 nm. According to Peng's empirical equations, the size of QDs1 and QDs2 were calculated about 3.43 nm and 2.50 nm (Yu et al., 2003), which were generally consistent with the above particle sizes. The band gap values of QDs1 and QDs2 could be calculated by the formula to be 2.0 and 2.3 eV, respectively (the detailed formula see Supplementary material).

### 3.3. Characterization of the biosensor platform

Cyclic voltammetry (CV) was an effective method for investigate the stepwise assembly processes of the electrode surface, which could characterize the fabrication process of the PEC biosensor at different stages in 5 mM $[Fe(CN)_6]^{3-/4-}$ solution containing 0.1 M KCl electrolyte. As shown in Fig. 3A, a well-defined redox peak was observed at the bare PWE (curve a). After the growth of Au NPs on the surface of PWE, the peak value significantly increased (curve b) due to the outstanding conductivity of Au NPs. Since the semiconductors have low conductivity, the CV response moderately reduced (curve c) after

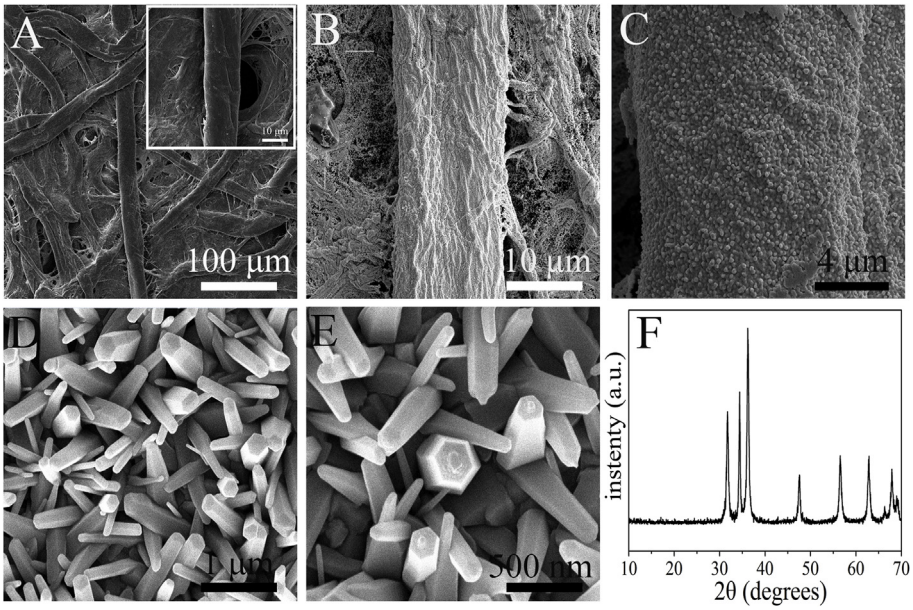


**Fig. 1.** SEM images of (A) bare paper (Inset: magnification SEM images of bare paper), (B, C) Au-PWE and (D, E) ZnO NRs; (F) XRD pattern of ZnO NRs.

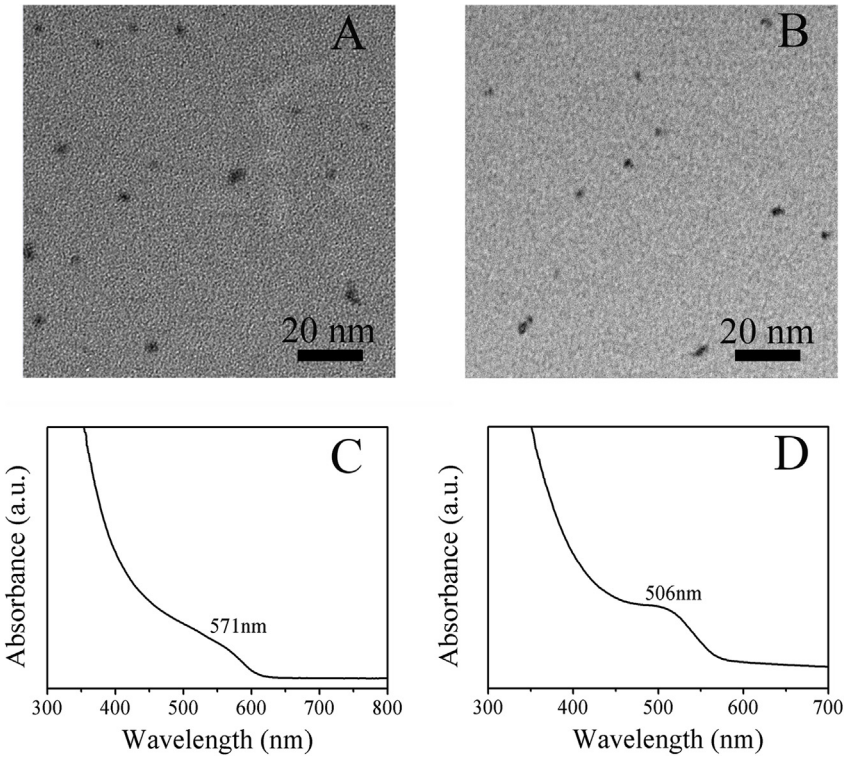


**Fig. 2.** TEM images of (A) QDs1 and (B) QDs2; UV-vis absorption spectra of (C) QDs1 and (D) QDs2.

sequentially connecting ZnO NRs and different sizes of CdTe QDs on the electrode surface. Subsequently, the CV response sequentially decreased (curve d) when H-DNA and ALP-Au NPs-DNA were introduced on the surface of the electrode, because the nucleic acid molecules and organic molecules with insulating property hindered the redox probe into the electrode surface. In the presence of T-DNA, the CV response increased (curve e) again because of the disassembly of triple-helix molecule compelled ALP-Au NPs-DNA to leave the electrode surface, which resulted in a decrease in steric hindrance.

The stepwise assembly processes of the PEC biosensor were further characterized by the electrochemical impedance spectroscopy (EIS). As shown in Fig. 3B, for the bare PWE, curve a displayed a relatively small resistance (Ret). Compared with the EIS of bare PWE, after the Au NPs were grown onto PWE, the Ret obviously decreased (curve b), which suggested that the Au NPs enhanced the conductivity of PWE. After ZnO NRs and different sizes of CdTe QDs were attached to the surface of Au-PWE, the corresponding Ret values slightly increased (curve c), suggesting that low conductivity of semiconductors mildly inhibit the transfer of the redox probe to the electrode surface. The Ret value dramatically increased (curve d) after H-DNA and ALP-Au NPs-DNA were immobilized on the surface of the electrode step by step, demonstrating that nucleic acid with insulating property would increase the steric hindrance and impede the access of the redox probe to the electrode surface. The Ret value decreased (curve e) due to the specific

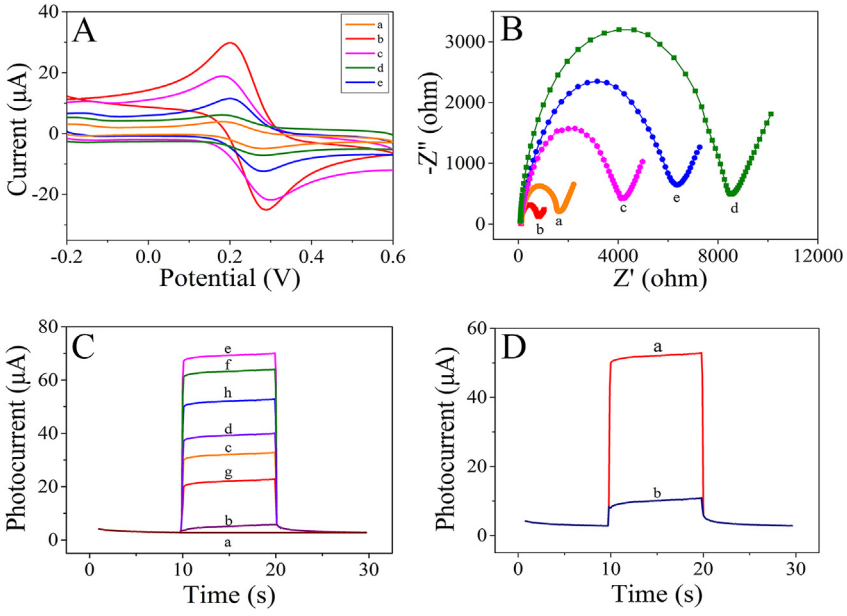


**Fig. 3.** (A) CV and (B) EIS of (a) bare PWE, (b) Au-PWE, (c) QDs2/QDs1/ZnO/Au-PWE, (d) ALP-Au NPs-DNA/H-DNA/QDs2/QDs1/ZnO/Au-PWE, (e) T-DNA/ALP-Au NPs-DNA/H-DNA/QDs2/QDs1/ZnO/Au-PWE in 5 mM $[Fe(CN)_6]^{3-/4-}$ solution containing 0.1 M KCl; (C) Photocurrent responses of (a) bare PWE, (b) Au-PWE, (c) ZnO/Au-PWE, (d) QDs1/ZnO/Au-PWE, (e) QDs2/QDs1/ZnO/Au-PWE, (f) H-DNA/QDs2/QDs1/ZnO/Au-PWE, (g) ALP-Au NPs-DNA/H-DNA/QDs2/QDs1/ZnO/Au-PWE, (h) T-DNA/ALP-Au NPs-DNA/H-DNA/QDs2/QDs1/ZnO/Au-PWE in PBS solution (pH 7.4) containing 0.1 M AA; (D) Photocurrent responses of (a) ALP-Au NPs-DNA/H-DNA/QDs2/QDs1/ZnO/Au-PWE, (b) T-DNA/ALP-Au NPs-DNA/H-DNA/QDs2/QDs1/ZnO/Au-PWE in PBS solution (pH 7.4) containing 0.1 M AAP.

hybridization of the obtained PEC biosensor with T-DNA to cause the decrease of steric hindrance. In view the consistent measurement results of CV and EIS, the successful construction of the designed PEC biosensor was confirmed.

### 3.4. PEC response of the biosensor platform

The PEC responses of the stepwise assembly processes were recorded in PBS solution (pH 7.4) containing 0.1 M AA. As shown in Fig. 3C, for bare PWE and Au-PWE, a small photocurrent response was observed (curves a and b). After the ZnO NRs were immobilized on the Au-PWE, the photocurrent response moderately increased (curve c), indicating that ZnO NRs could absorb ultraviolet light and accelerate the electrons transfer process. After the QDs1 and QDs2 were further modified on the ZnO/Au-PWE, the photocurrent response significantly increased (curves d and e) because the different sizes of CdTe QDs could harvest longer wavelength light and further promote the electrons transfer, which verified that the cascaded structure effectively increased the photocurrent response. When the H-DNA was immobilized on the electrode surface, the photocurrent response slightly decreased (curve f), suggesting the nucleic acid molecule hindered the electron transfer between the electron donors and the electrode surface. After the ALP-Au NPs-DNA was modified on the electrode surface, the photocurrent response sequentially decreased (curve g), because the increase of the steric hindrance further hindered the combination of electrons with holes. When T-DNA was added, the photocurrent response increased again (curve h), since the steric hindrance was reversely reduced due to the disassembly of triple-helix conformation forcing ALP-Au NPs-DNA to be away from the electrode surface. The change of photocurrent responses in each stages suggested that the proposed biosensor had excellent feasibility.

The T-DNA specific detection was based on the photocurrent response change resulted from conformation change of the triple-helix molecule after hybridization with T-DNA. Scheme 2 showed the photocurrent generation mechanism of the PEC biosensor based on cascaded photoactive materials and triple-helix molecular switch. As shown in Fig. 3D, in the absence of T-DNA, the triple-helix molecule was in a closed state and the ALP of ALP-Au NPs-DNA could specifically catalyze the AAP to generate AA as electron donors, which led to a very strong photocurrent response (curve a) due to the rapid electrons transfer process. However, in the presence of T-DNA, the T-DNA hybridized with ALP-Au NPs-DNA molecules, which caused triple-helix molecule in an opened state and compelled ALP-Au NPs-DNA away from the electrode surface, resulting in the absence of ALP which could catalyze AAP to generate AA. Subsequently, the photocurrent response significantly decreased (curve b). Accordingly, the decrease of photocurrent response indicated that the proposed biosensor was built as expect.

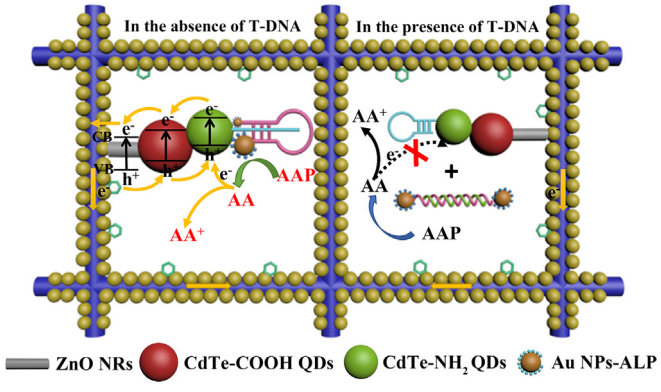


**Scheme 2.** Schematic illustration of the electron – holes transfer process of the PEC biosensor based on cascaded photoactive materials and triple-helix molecular switch.

### 3.5. PEC detection for T-DNA

Under the optimal conditions (Fig. S2), the photocurrent intensity was closely associated with the concentration of T-DNA. The linear curve was measured by varying the concentration of T-DNA, and the results were presented in Fig. 4A. As the increment of T-DNA concentration, the photocurrent responses continuously decreased, owing to the gradually decreasing quantity of ALP-Au NPs-DNA on the electrode surface with the concentration of T-DNA increased, which reduced the generation of AA as electron donors. The photocurrent responses linearly decreased with increasing logarithm of T-DNA concentration in the range from 1 fM to 1 nM (Fig. 4B). The linear equation was $I = 10.42–2.11 \log C_{T\text{-}DNA}$ with a good linear coefficient of 0.9901. The limit of detection (LOD, S/N = 3) was calculated to be 0.65 fM. It could be proved that the proposed biosensor possessed outstanding performance. Table S2 showed the performance of DNA detection in contrast to other works. The superiority of the proposed biosensor could be seen clearly.

### 3.6. Reproducibility, specificity, stability of PEC biosensor

The reproducibility of the developed PEC biosensor is estimated on the basis of intra-assay and inter-assay relative standard deviations (RSDs). The intra-assay RSD value was 4.1% by detecting 1 pM of T-DNA with five parallel experiments. The RSD value of the inter-assay is 4.7% by using five working electrodes fabricated under the identical experimental conditions to incubate with 1 pM of T-DNA. Above results greatly revealed that the PEC biosensor possessed a favorable reproducibility and precision.

Specificity is an essential criterion for the property of the PEC biosensor. The effect of different DNA sequences, such as T-DNA, single-base mismatched DNA (Sm-DNA), three-base mismatched DNA (Tm-DNA) and non-complementary DNA (N-DNA) on the photocurrent changes were investigated. To verify the specificity of the designed PEC biosensor, experiments were performed on the same concentration of the above DNA sequences. As shown in Fig. 4C, comparing to the blank test, the photocurrent response was reduced significantly when incubated with T-DNA. With the number of mismatch base sequences increased, the photocurrent responses increased continuously, which revealed that the designed biosensor had an excellent specificity.

Stability is also critical for the biosensor. After the PEC biosensor was stored in a dark and humid environment at 4 °C over 4 weeks, as shown in Fig. 4D, the photocurrent response maintained 88.3% of its original response, demonstrating the excellent stability of the PEC biosensor.

### 3.7. Feasibility of the proposed PEC biosensor

To evaluate the feasibility and potential application in real sample, the experiments were carried out via using PEC biosensor to monitor HIV-1 levels in human serum samples from healthy individuals. Different concentrations of HIV-1 were added to serum samples and diluted to a certain concentration with pH 7.4 PBS, the recoveries of HIV-1 were determined to be 97.6–101.8% (Table S3). Through the above results, proving the PEC biosensor possessed excellent feasibility in real sample and had great potential in practical applications.

## 4. Conclusion

In summary, a simple, low-cost and selective PEC biosensor was fabricated for ultrasensitive detection of HIV-1 based on cascaded photoactive materials and triple-helix molecular switch. ZnO NRs and different sizes of CdTe QDs were adopted to form a cascaded photoactive interface to achieve signal amplification. The presence of T-DNA

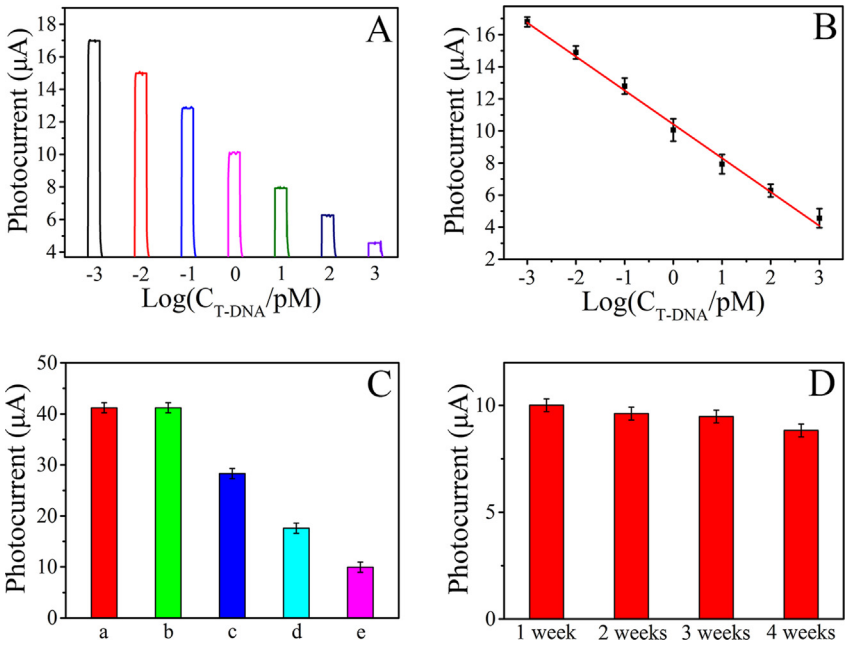


**Fig. 4.** (A) Photocurrent responses and (B) calibration curve of the PEC biosensor for the detection of different concentrations of T-DNA from 1 fM to 1 nM. The error bars showed the standard deviation of five replicate determinations; (C) Photocurrent responses of the PEC biosensor with different sequences of T-DNA (20 μL, 1 pM): (a) Blank, (b) N-DNA, (c) Tm-DNA, (d) Sm-DNA, (e) T-DNA. The error bars showed the standard deviation of five independent experiments; (D) Photocurrent responses of the PEC biosensor at different storage times. PEC tests were performed in PBS solution (pH 7.4) containing 0.1 M AAP with a constant potential of 0.0 V and Xe lamp as the light source.

disassembled the triple-helix conformation on the surface of the biosensor to compel ALP-Au NPs-DNA leave the electrode surface to decrease the photocurrent response evidently. The superiority of triple-helix molecular switch opened up a new strategy for highly specificity detection of T-DNA. Compared to other biosensors, the proposed paper-based PEC biosensor exhibited better reproducibility, specificity, stability and offered a lower detection limit (0.65 fM). It is worth mentioning that the PEC biosensor could detect any targets by changing the DNA sequence of ALP-Au NPs-DNA. However, the designed biosensor cannot visually detect the target molecule. To achieve the goal, we will focus on constructing a visual biosensor on a paper-based analytical device in the future work.

## CRediT authorship contribution statement

**Shaopeng Wang:** Conceptualization, Methodology, Writing - original draft. **Jinge Zhao:** Investigation, Formal analysis. **Yan Zhang:** Visualization, Data curation. **Mei Yan:** Resources, Visualization. **Lina Zhang:** Writing - review & editing, Resources. **Shenguang Ge:** Conceptualization, Supervision, Funding acquisition. **Jinghua Yu:** Funding acquisition, Project administration.

## Acknowledgements

This work was financially supported by the National Natural Science Foundation of China (21575051, 21775055, 21874055); the Key Research and Development Program of Shandong Province, China (2018GGX103037); The project of "20 items of University" of Jinan (No. 2018GXRC001); Major Program of Shandong Province Natural Science Foundation (ZR2017ZC0124) and the Taishan Scholars Program (ts201712048).

## Appendix A. Supplementary data

Supplementary data to this article can be found online at https://doi.org/10.1016/j.bios.2019.111325.

## References

Baeissa, A., Dave, N., Smith, B.D., Liu, J., 2010. ACS Appl. Mater. Interfaces 2 (12), 3594–3600.
Chai, Y., Tian, D., Wang, W., Cui, H., 2010. Chem. Commun. 46 (40), 7560–7562.
Chen, J., Zhang, J., Guo, Y., Li, J., Fu, F., Yang, H.H., Chen, G., 2011. Chem. Commun. 47 (28), 8004–8006.
Darain, F., Park, S.-U., Shim, Y.-B., 2003. Biosens. Bioelectron. 18 (5), 773–780.
Fan, G.C., Han, L., Zhang, J.R., Zhu, J.J., 2014. Anal. Chem. 86 (21), 10877–10884.
Fan, G.C., Zhu, H., Du, D., Zhang, J.R., Zhu, J.J., Lin, Y., 2016. Anal. Chem. 88 (6), 3392–3399.
Feng, Y., Zhang, H., Guan, Y., Mu, Y., Wang, Y., 2017. J. Power Sources 348, 246–254.
Ge, L., Wang, W., Sun, X., Hou, T., Li, F., 2016. Anal. Chem. 88 (19), 9691–9698.
Gill, R., Zayats, M., Willner, I., 2008. Angew. Chem. Int. Ed. 47 (40), 7602–7625.
Haddour, N., Chauvin, J., Gondran, C., Cosnier, S., 2006. J. Am. Chem. Soc. 128 (30), 9693–9698.
Hu, R., Liu, T., Zhang, X.-B., Huan, S.-Y., Wu, C., Fu, T., Tan, W., 2014. Anal. Chem. 86 (10), 5009–5016.
Huang, J., Su, X., Li, Z., 2012. Anal. Chem. 84 (14), 5939–5943.
Ito, T., Hosokawa, K., Maeda, M., 2007. Biosens. Bioelectron. 22 (8), 1816–1819.
Lan, F., Sun, G., Liang, L., Ge, S., Yan, M., Yu, J., 2016. Biosens. Bioelectron. 79, 416–422.
Lee, Y.-L., Chi, C.-F., Liau, S.-Y., 2010. Chem. Mater. 22 (3), 922–927.
Li, C., Wang, H., Shen, J., Tang, B., 2015. Anal. Chem. 87 (8), 4283–4291.
Li, F., Du, Z., Yang, L., Tang, B., 2013. Biosens. Bioelectron. 41, 907–910.
Li, L., Zhang, Y., Zhang, L., Ge, S., Liu, H., Ren, N., Yan, M., Yu, J., 2016. Anal. Chem. 88 (10), 5369–5377.
Li, R., Zhang, Y., Tu, W., Dai, Z., 2017. Appl. Mater. Interfaces 9 (27), 22289–22297.
Liu, S., Lin, Y., Wang, L., Liu, T., Cheng, C., Wei, W., Tang, B., 2014. Anal. Chem. 86 (8), 4008–4015.
Ma, C., Wang, W., Li, Z., Cao, L., Wang, Q., 2012. Anal. Biochem. 429 (2), 99–102.
Patterson, A., Caprio, F., Vallée-Bélisle, A., Moscone, D., Plaxco, K.W., Palleschi, G., Ricci, F., 2010. Anal. Chem. 82 (21), 9109–9115.
Qian, Z., Bai, H.-J., Wang, G.-L., Xu, J.-J., Chen, H.-Y., 2010. Biosens. Bioelectron. 25 (9), 2045–2050.
Sauna, Z.E., Kimchi-Sarfaty, C., 2011. Nat. Rev. Genet. 12, 683.
Shu, J., Qiu, Z., Lv, S., Zhang, K., Tang, D., 2018. Anal. Chem. 90 (4), 2425–2429.
Tang, J., Kong, B., Wang, Y., Xu, M., Wang, Y., Wu, H., Zheng, G., 2013. Nano Lett. 13 (11), 5350–5354.
Wang, X., Jiang, A., Hou, T., Li, F., 2014. Analyst 139 (23), 6272–6278.
Wang, X., Jiang, A., Hou, T., Li, F., 2015. Anal. Chim. Acta 890, 91–97.
Yu, W.W., Qu, L., Guo, W., Peng, X., 2003. Chem. Mater. 15 (14), 2854–2860.
Zang, Y., Lei, J., Zhang, L., Ju, H., 2014. Anal. Chem. 86 (24), 12362–12368.
Zhang, H.-R., Xu, J.-J., Chen, H.-Y., 2013. Anal. Chem. 85 (11), 5321–5325.
Zhang, K., Lv, S., Lin, Z., Tang, D., 2017. Biosens. Bioelectron. 95, 34–40.
Zhang, L., Li, D., Meng, W., Huang, Q., Su, Y., Wang, L., Song, S., Fan, C., 2009. Biosens. Bioelectron. 25 (2), 368–372.
Zhang, Y., Ge, L., Li, M., Yan, M., Ge, S., Yu, J., Song, X., Cao, B., 2014. Chem. Commun. 50 (12), 1417–1419.
Zhang, Y., Tang, Z., Wang, J., Wu, H., Maham, A., Lin, Y., 2010. Anal. Chem. 82 (15), 6440–6446.
Zhao, W.-W., Xu, J.-J., Chen, H.-Y., 2018. Anal. Chem. 90 (1), 615–627.
Zhao, W.W., Ma, Z.Y., Yan, D.Y., Xu, J.J., Chen, H.Y., 2012. Anal. Chem. 84 (24), 10518–10521.
Zheng, J., Jiao, A., Yang, R., Li, H., Li, J., Shi, M., Ma, C., Jiang, Y., Deng, L., Tan, W., 2012. J. Am. Chem. Soc. 134 (49), 19957–19960.